
Article:
Ogasawara, Takahiro, Kim, Jun-Young orcid.org/0000-0002-1639-3270, Ando, Yasuo et al. (1 more author) (2018) Structural and antiferromagnetic characterization of noncollinear D019 Mn3Ge polycrystalline film. Journal of Magnetism and Magnetic Materials. pp. 7-11. ISSN 0304-8853

https://doi.org/10.1016/j.jmmm.2018.10.035

Journal of Magnetism and Magnetic Materials 473 (2019) 7–11

Contents lists available at ScienceDirect

Journal of Magnetism and Magnetic Materials

journal homepage: www.elsevier.com/locate/jmmm

Research articles

Structural and antiferromagnetic characterization of noncollinear $D0_{19}$ Mn_3Ge polycrystalline film

Takahiro Ogasawara[a,b], Jun-young Kim[c,*], Yasuo Ando[a,d,e,*], Atsufumi Hirohata[b]

[a] Department of Applied Physics, Graduate School of Engineering, Tohoku University, Sendai 980-8579, Japan
[b] Department of Electronic Engineering, University of York, Heslington YO10 5DD, United Kingdom
[c] Department of Physics, University of York, Heslington YO10 5DD, United Kingdom
[d] Center for Science and Innovation in Spintronics (Core Research Cluster) Organization for Advanced Studies, Japan
[e] Center for Spintronics Research Network, Tohoku University, Sendai 980-8579, Japan

ABSTRACT

Distorted Heusler compound of $D0_{19}$ Mn_3Ge polycrystalline films were studied in terms of their crystalline structures and antiferromagnetic behavior by varying annealing temperature and Mn-Ge composition. Although low temperature growth for 30 nm Mn_3Ge showed no diffraction peaks in X-ray diffraction patterns, high temperature growth over 773 K with Mn-rich composition is found to promote the (0001) orientation of $D0_{19}$ Mn_3Ge which resulted in the emergence of an exchange bias effect in $Co_{0.6}Fe_{0.4}$ ferromagnetic layer at 120 K. The exchange bias field of 12 Oe in $Mn_{3.16}Ge$ film grown at 773 K were improved to 61 Oe by enriching Mn composition to $Mn_{3.97}Ge$. The average blocking temperature was measured to be at 150 K which is not as high as its reported Néel temperature of 390 K in the bulk state, however, further improvements are expected by doping additional transition elements.

Exchange bias effect induced at the interface between antiferromagnetic and ferromagnetic layers has played an important role as a building block of the spintronic devices to pin the magnetization of ferromagnetic layer. After the first discovery of the exchange bias effect from CoO [1], many antiferromagnetic materials have been found such as IrMn which has been most commonly used as an antiferromagnetic material for the device applications such as a spin-valve structure [2]. However, new antiferromagnetic materials should be developed for the replacement of IrMn due to the depletion of Ir being identified as a critical raw metal [3]. From this view point, antiferromagnetic binary Heusler alloys such as the $D0_{19}$ Mn_3Z (Z = Ga [4–7], Ge [8] and Sn [9]) have been studied on their structural and magnetic properties. As an Mn_3Ge binary alloy is taken as an example, it allows two stable crystalline structures of the tetragonal $D0_{22}$ and hexagonal $D0_{19}$ structures which is distorted from the basic full-Heusler $L2_1$ structures along the (0 0 1) and (1 1 1) direction, respectively [10]. As a result of different crystalline structures, the $D0_{22}$ or $D0_{19}$ structure exhibits different magnetic anisotropy such as ferrimagnet with perpendicular magnetic anisotropy and low saturation magnetization [11,12] or antiferromagnet with noncollinear magnetic moments in which exchange bias effect [8] or giant anomalous hall effect [13,14] are appeared. In the bulk state, the $D0_{19}$ phases are formed by high temperature annealing according to the Mn-Ge phase diagram [15,16]. Fig. 1 shows the crystalline structure of $D0_{19}$ Mn_3Ge with 6 Mn and 2 Ge atoms in a unit cell. Lattice constants are calculated to be a = 5.28 Å and c = 4.22 Å [10], and experimentally measured to be a = 5.34 Å and c = 4.32 Å [8], respectively. In the *ab* plane, Kagome lattice, *i.e.*, triangular configuration of Mn atoms, are formed [17]. This sublattice results in geometrical frustration of magnetic moments, which are stabilized by the Dzyaloskinskii-Moriya interaction [17–19]. Consequently, each Mn magnetic moment is aligned triangular 120° direction along the *ab* plane and shows antiferromagnetic behavior with the Néel temperature, T_N of 390 K [20] at which antiferromagnetic order disappears. Owing to this noncollinear configuration of magnetic moment, weak ferromagnetism with the Currie temperature T_c, at 365 K [21] and a magnetic moment of 0.005–0.008 μ_B per Mn atom, where μ_B denotes Bohr magneton, are demonstrated by previous experiments [13,14]. Although $D0_{19}$ Mn_3Ge has been studied in the bulk state, for the further understandings and spintronic applications, its structural and magnetic characterizations in the thin film form are necessary. Therefore, we focus on the exchange bias effect induced from antiferromagnetic Mn_3Ge thin films. Successfully we demonstrate to grow $D0_{19}$ $Mn_{3.16}Ge$ films with substrate heating which exhibits the exchange bias up to 13 Oe at 120 K. In addition, the exchange bias is found to be improved by doping additional Mn atoms up to 64 Oe because of the improved (0001) orientation of Mn_3Ge.

All the polycrystalline samples were fabricated using a Plasma Quest high target utilization sputtering (HiTUS) system with a base

* Corresponding authors.
E-mail addresses: takahiro.ogasawara.p3@dc.tohoku.ac.jp (T. Ogasawara), junyoung.kim@york.ac.uk (J.-y. Kim), ando@mlab.apph.tohoku.ac.jp (Y. Ando), atsufumi.hirohata@york.ac.uk (A. Hirohata).

https://doi.org/10.1016/j.jmmm.2018.10.035
Received 27 July 2018; Received in revised form 7 October 2018; Accepted 8 October 2018
Available online 09 October 2018

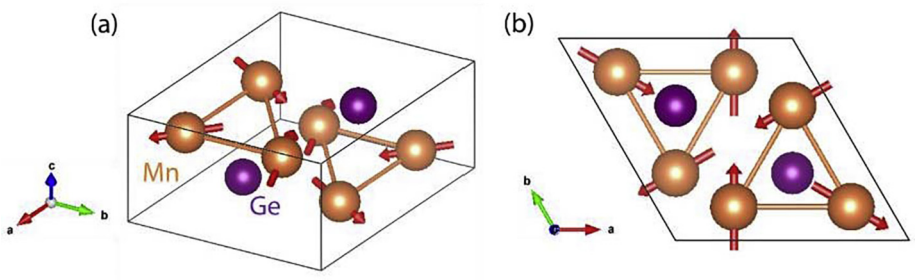

Fig. 1. Illustration of the $D0_{19}$ Mn_3Ge structure. Red arrows describe expected Mn moment directions. (For interpretation of the references to colour in this figure legend, the reader is referred to the web version of this article.)

pressure less than 5×10^{-5} Pa. The stacking structures of Ta (5)/Ru (35)/Mn_3Ge (30)/$Co_{0.6}Fe_{0.4}$ (0 or 3.3)/Ta (5) (thickness in nm) were grown onto Si (0 0 1) substrate in 1.86 mbar Ar atmosphere with a bias voltage of −900 V to maximize grain volume [22] (hereinafter refer to $Co_{0.6}Fe_{0.4}$ as CoFe). The sputtering rate of Mn_3Ge is *ca.* 0.8 Å/s. For the film growth, different heating treatments were carried out such as substrate heating for the growth of Mn_3Ge at T_s or *ex-situ* post-annealing at T_a in a range of 573–823 K by using heater lamp located above a substrate in the chamber. The Mn-Ge compositions were also controlled from $Mn_{2.67}Ge$ to $Mn_{3.97}Ge$, respectively by adding Mn pegs into Mn_3Ge target. The compositions were measured using energy dispersive X-ray spectroscopy (EDX). The crystalline structures and magnetic properties were characterized by X-ray diffraction (XRD; Rigaku, Smart Lab) at room temperature (RT) and vibrating sample magnetometer (VSM; ADE, Model 10) between 100 and 300 K.

Fig. 2(a) shows XRD spectra of 2θ scan for the films with the stacking of Ta (5)/Ru (35)/$Mn_{3.80}Ge$ (30)/CoFe (3.3)/Ta (5) (thickness in nm) post-annealed at various T_a. For the films post-annealed at the temperature range between RT and 673 K, there is no peak associated with Mn_3Ge appeared in the XRD spectra. It should be noted that the sharp peaks shown at $2\theta = ca.$ 33° are originated from misalignment of a Si substrate. However, as increasing T_a above 773 K, the films exhibit $D0_{19}$ Mn_3Ge (20$\bar{2}$1) and (40$\bar{4}$2) peaks. This behavior may be caused by the formation of the $D0_{19}$ phase of Mn_3Ge which is the higher temperature phase than the $D0_{22}$ phase in the bulk state. Also, the (20$\bar{2}$1) peak intensity is the highest in accordance with calculated and experimental results as previously reported [8]. On the other hand, as shown in Fig. 2(b), a substrate-heated sample during Mn_3Ge deposition shows a different crystalline orientation. The films with the stacking of Ta (5)/Ru (35)/$Mn_{3.16}Ge$ (30)/CoFe (3.3)/Ta (5) (thickness in nm) grown at T_s below 573 K show no peak similarly to Fig. 2(a). However, the peaks from $D0_{19}$ Mn_3Ge (0002) and (0004) planes as well as (20$\bar{2}$1) and (40$\bar{4}$2) planes are visible with T_s over 723 K. Although they are overlapped with the Ru (0002) peak, the presence of diffractions at a higher angle confirms the peak identification. As a result, it suggests the films with T_s over 723 K are crystallized with the mixture of the (0001) and (20$\bar{2}$1) orientations normal to the film plane. The (0001) orientation of $D0_{19}$ Mn_3Z is favorable to induce the exchange bias as previously reported [5,7,9], indicating that the substrate-heated samples are advantageous than the post-annealed samples for this purpose. The lattice constants of the $Mn_{3.16}Ge$ with T_s = 773 and 823 K are estimated to be a = 5.53 Å and c = 4.32 Å, and a = 5.54 Å and c = 4.33 Å, respectively, from clearly distinctive (0004) and (20$\bar{2}$1) peaks. This minor distortion in the *ab* plane is associated with the lattice mismatch of 1.3% with the Ru buffer layer. The magnetization curve of 30-nm-thick $Mn_{3.16}Ge$ at T_s = 773 K measured at RT is shown in Fig. 3. The weak ferromagnetic behavior is shown similarly to previous bulk studies [13,14]. The hysteresis in this figure indicates the spin chirality switching of triangular Mn atoms [23]. The small saturation magnetization M_s is estimated to be 34 emu/cm^3 which value is approximately the same with previous work of Mn_3Sn film [9]. However, the magnetic

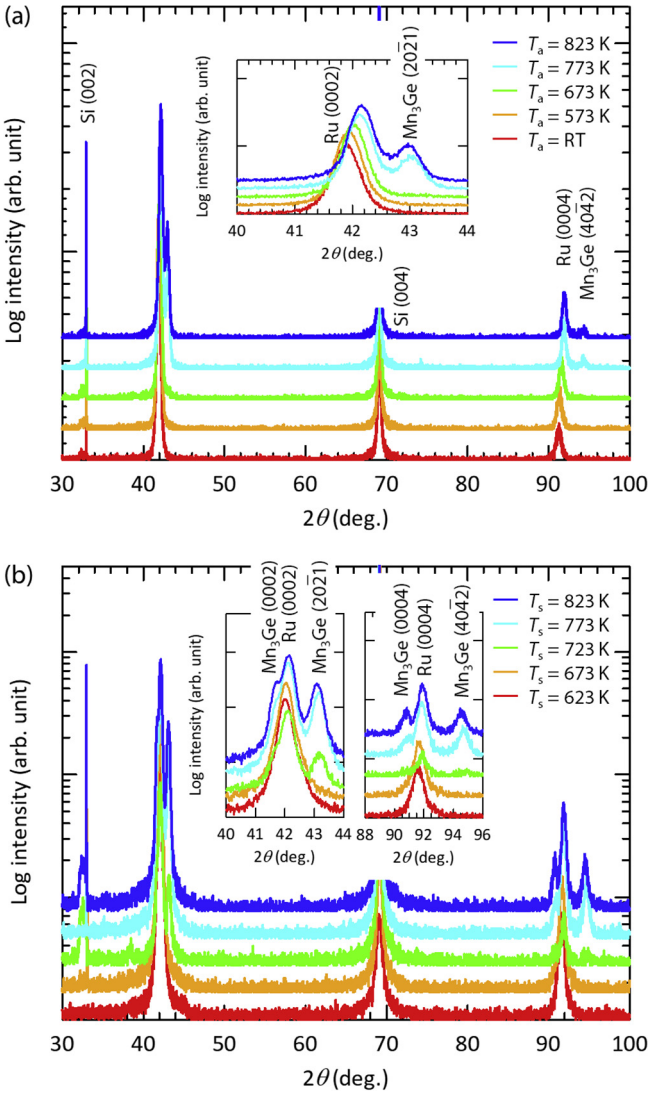

Fig. 2. XRD spectra of the 2θ scans for the 30-nm-thick (a) $Mn_{3.80}Ge$ films with *ex-situ* post-annealing at T_a, and (b) $Mn_{3.16}Ge$ films with substrate heating at T_s.

moment per Mn in this film is estimated to be 0.06 μ_B, which is almost 10 times higher than that in the Mn_3Ge bulk state with 0.005–0.008 μ_B [13,14]. In general, such a small net magnetic moment of Mn_3Ge is associated with the formation of the Kagome lattice with 3 Mn atoms which leads canting of Mn moments [13,14]. However, once Mn atoms occupy Ge sites, the triangular moment configuration cannot be formed which results in a larger net moment. Therefore, this increase of magnetic moment is attributed to excess Mn atoms which occupy Ge sites randomly. Another possible reason is random grain orientations owing

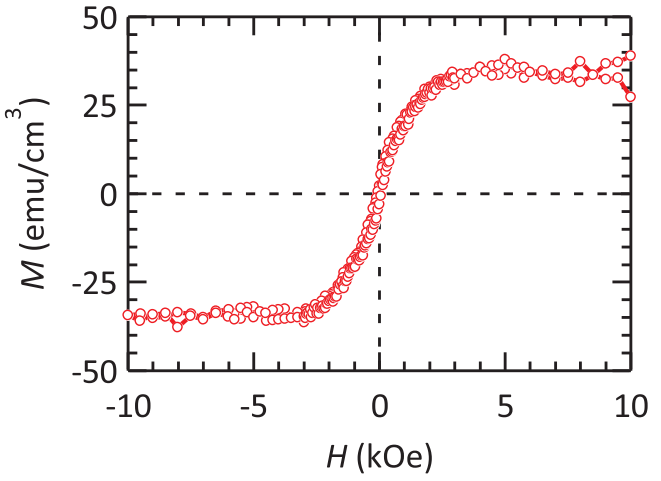

Fig. 3. In-plane magnetization curve of the 30-nm-thick $Mn_{3.16}Ge$ film grown at T_s = 773 K measured at RT.

to the polycrystalline nature of our films which causes less interactions of triangular Mn moments at the grain boundaries.

The exchange bias, H_{ex}, originated at the interface between $Mn_{3.16}Ge$/CoFe was measured from the shift of hysteresis loop. H_{ex} was induced by field cooling down to 100 or 120 K after the samples were annealed at 500 K for 30 mins with an external in-plane magnetic field of −6 kOe. Fig. 4 displays magnetization curves of $Mn_{3.16}Ge$/CoFe bi-layers grown at T_s = 773 K measured at 100 and 120 K. Both curves show positive horizontal shift which indicates the existence of exchange coupling at the interfaces and H_{ex} is estimated to be at 28 and 12 Oe at 100 and 120 K, respectively. The observed exchange bias in this film is lower than the other Mn_3Z films (Z = Ga [5,7] and Sn [9]) due to the mixture of the (0001) and $(20\bar{2}1)$ crystalline orientations. In addition, Fig. 5 shows the results of X-ray reflectivity (XRR) of the $Mn_{3.16}Ge$/CoFe (3.3) film. Sample information such as thickness and density is used for fitting of the measured reflectivity which results in Ta (3.4 ± 0.3)/Ru (35.7 ± 0.6)/$Mn_{3.16}Ge$ (30.7 ± 1.9)/CoFe (3.73 ± 1.1)/Ta (4.0 ± 0.2) (thickness in nm). This large roughness in the $Mn_{3.16}Ge$ layer is also one of the possible reasons to decrease the exchange bias.

Next, we studied the Mn-Ge composition effect on the film growth and exchange bias effect. Fig. 6 shows XRD diffraction patterns of Ta (5)/Ru (35)/Mn_xGe (30)/CoFe (3.3)/Ta (5) (thickness in nm) with T_s = 773 K. In this graph, a large Mn composition increases the

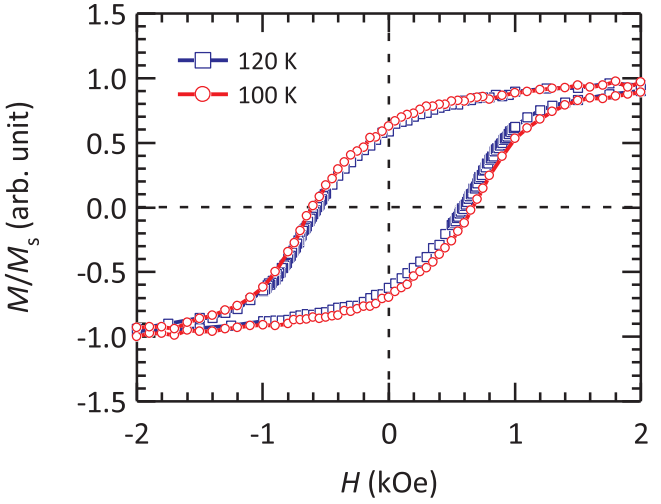

Fig. 4. In-plane magnetization curves of the $Mn_{3.16}Ge$ (30)/CoFe (3.3) film measured at 100 K and 120 K after field cooling.

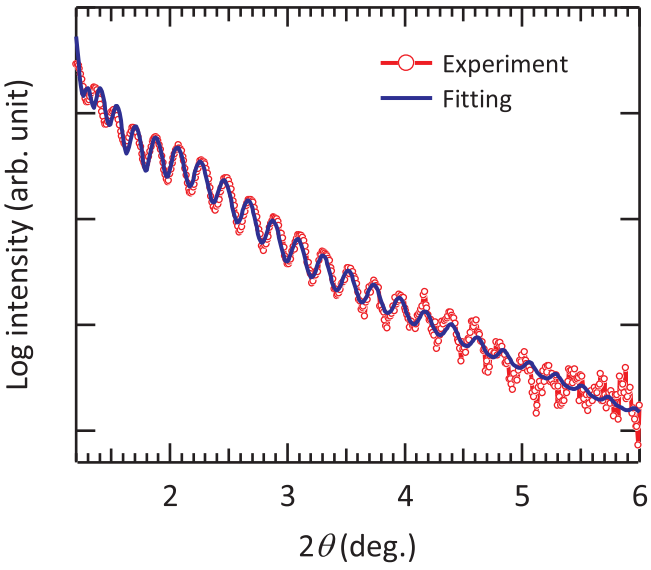

Fig. 5. X-ray reflectivity of the $Mn_{3.16}Ge$ (30)/CoFe (3.3) film grown at T_s = 773 K.

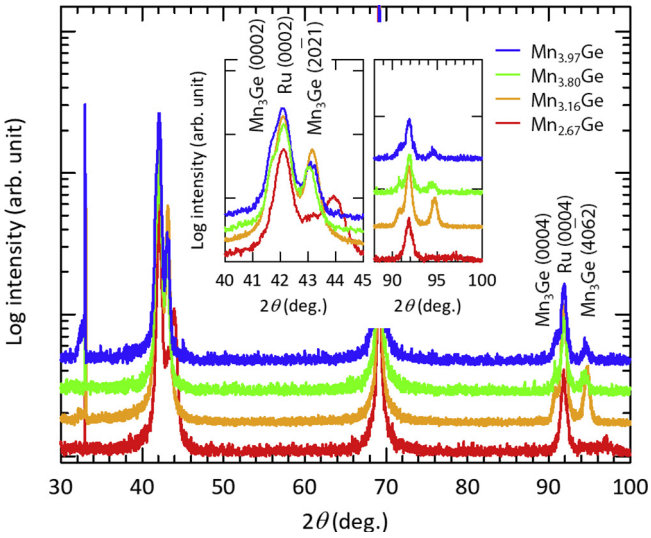

Fig. 6. XRD spectra of the 2θ scans for the 30-nm-thick Mn_xGe films grown at T_s = 773 K.

intensity of the (0002) peak while that of the $(20\bar{2}1)$ peak is suppressed. The lattice constant of $Mn_{3.97}Ge$ is determined to be a = 5.53 Å and c = 4.32 Å, respectively, which is the same with the $Mn_{3.16}Ge$ film as described above. However, the atomic radius of Mn, 1.27 Å is larger than that of Ge, 1.22 Å, and hence, the large Mn compositions increase the in-plane lattice constant of Mn_3Ge. Therefore, $Mn_{3.97}Ge$ may experience less frustration than $Mn_{3.16}Ge$ during the growth onto the (0001) plane of the Ru buffer layer, resulting in the promotion of the $D0_{19}$ (0001) orientation. In order to confirm the antiferromagnetic behavior, the exchange bias were measured in these structures. Fig. 7(a) displays magnetization curves of Mn_xGe (30)/CoFe (3.3) layered film measured at 120 K and, while Fig. 7(b) shows H_{ex} dependent on the Mn composition, x. Horizontal shift of magnetization curves are shown for the film of Mn_xGe with x above 3.16. $Mn_{2.67}Ge$ does not have the (0001) orientation as shown in Fig. 6. Hence, the exchange bias are almost zero. With increasing Mn composition, the exchange bias is found to be increased gradually up to 61 Oe in the film of $Mn_{3.97}Ge$, while the (0001) orientation of $D0_{19}$ Mn_3Ge becomes dominant as compared with the $(20\bar{2}1)$ orientation. It should be noted that the

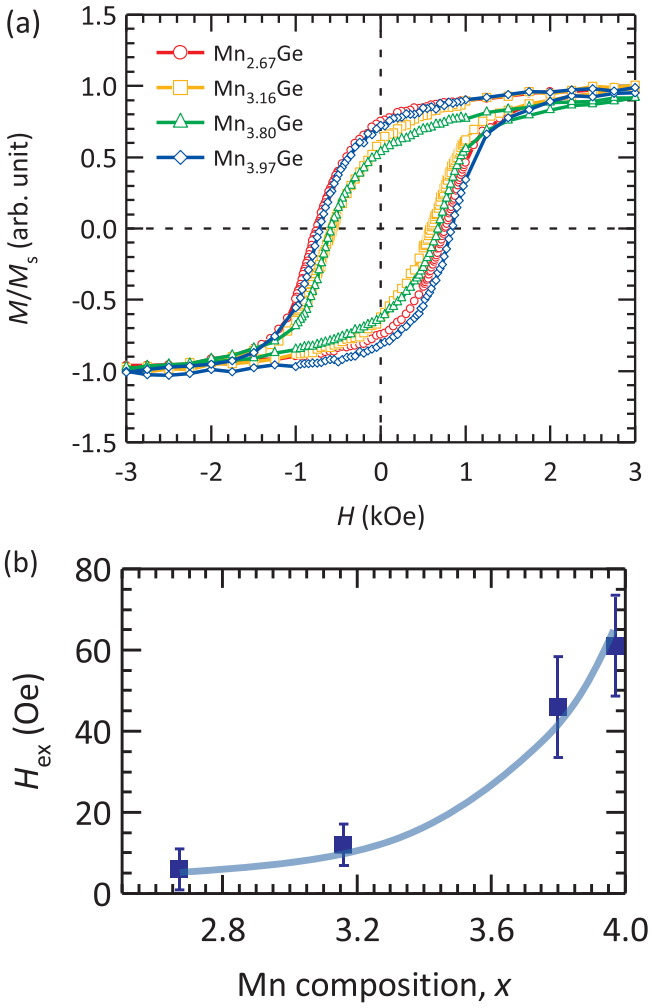

Fig. 7. (a) In-plane magnetization curves of Mn_xGe (30)/CoFe (3.3) films grown at T_s = 773 K measured at 120 K. (b) H_{ex} dependence on Mn composition, x. The line is guide to eyes.

vertical magnetization shift of 27 emu/cm^3 from the saturated magnetization, M_s, of 1180 emu/cm^3 is observed in a $Mn_{3.97}Ge$/CoFe bilayer, which is more than twice larger than that for $Mn_{3.16}Ge$, 12 emu/cm^3. This vertical shift is associated with increased interfacial uncompensated spins [24], which can also contribute to the enhancement of the exchange bias.

In the thin films with antiferromagnet/ferromagnet bilayer, the temperature at which the exchange bias field becomes zero, *i.e.*, blocking temperature, T_B, is basically lower than T_N because of a finite size effect [25,26]. Accordingly the experimental determination of T_B is one of the important studies for antiferromagnetic films. Especially for the polycrystalline films, grain size of an antiferromagnet is distributed which results in that each grain with different sizes shows different T_B. According to the earlier study on the correlation between the exchange bias and the grain volume [27], the grain volume of a polycrystalline antiferromagnetic film predominantly controls the exchange bias properties. A polycrystalline film is formed by a large number of fine crystals, hence, the grain volume are varied following lognormal distribution. There are two critical volumes for the magnitude of exchange bias in such grain distribution. The first one is critical volume, V_c, below which the exchange bias cannot be set in grains below because they are thermally unstable. The second one is V_{set}, above which anisotropy energy is too high to induce the exchange bias. Therefore, the exchange bias can be set only in medium-sized grains between V_c and V_{set} [27,28]. Therefore, we carried out our T_B measurement by following

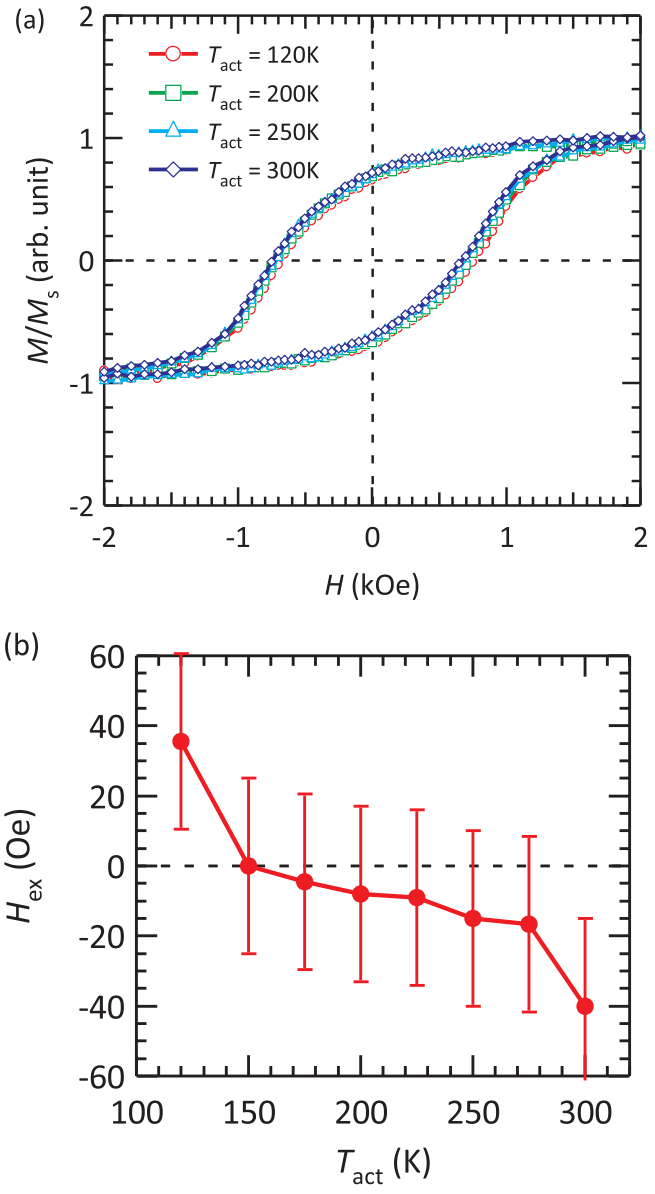

Fig. 8. (a) In-plane magnetization curves of $Mn_{3.97}Ge$ (30)/CoFe (3.3) with different activation temperature, T_{act} from 120 to 300 K measured at 120 K. (b) H_{ex} dependence as a function of T_{act}.

the York Protocol [28] which allowed us to determine average blocking temperature $\langle T_B \rangle$ among all of the grains. In this study, the samples were set at T_{set} = 500 K for 90 mins under an external magnetic field of −6 kOe to induce the exchange bias. Afterwards, the samples were heated at different activation temperature, T_{act}, for 30 mins with a reversed magnetic field of 6 kOe. T_{act} was elevated from 120 to 300 K at each thermal activation process. This process reverses the antiferromagnetic ordering of some distributed grains depending on T_{act}. As T_{act} becomes higher, larger antiferromagnetic grains are reversed owing to the thermal activation with a reversed magnetic field which are caused by elevated thermal energy exceeding energy barrier of ΔE standing for the stability of the antiferromagnetic grains [27,28]. Just after completing the thermal activation at each T_{act}, the samples were cooled back to 120 K, where the corresponding magnetization curve was measured to detect the modification of the exchange bias due to thermal activation process. Fig. 8(a) shows magnetization curves of a $Mn_{3.97}Ge$ (30)/CoFe (3.3) (thickness in nm) bilayer measured at 120 K after elevating activation temperature by following the procedure of the York Protocol. At T_{act} = 120 K, positive shift of the magnetization curve

is shown in the film because of the field cooling with a negative magnetic field. The exchange bias is shifted towards the negative field direction with increasing T_{act} since elevated T_{act} can reverse the antiferromagnetic ordering of some grains, which is *i.e.* thermal activation. As a result, H_{ex} dependent on T_{act} shows a gradual change as shown in Fig. 8(b). When T_{act} is around 150 K, a half of the antiferromagnetic ordering of set grains are reversed, which brings T_{act} to zero. This temperature is called the average blocking temperature of $\langle T_B \rangle$. When T_{act} is 300 K, as the absolute value of the exchange bias becomes almost the same as the initial measurement of 120 K, it suggests that almost all set grains are reversed. This experimental $\langle T_B \rangle$ of 150 K is much lower than T_N of bulk Mn_3Ge as high as 390 K [20]. This seems to be caused by excess Mn atoms occupying Ge site randomly. Moreover, from structural viewpoints, a polycrystalline film shows no in-plane texture, so that the (0001) oriented grains are grown without in-plane ordering. The Mn_3Ge film also consists of both the (0001) and $(20\bar{2}1)$ oriented antiferromagnetic grains. These two facts implying that the interactions between the Kagome lattices become almost random at the boundary of the grains results in low $\langle T_B \rangle$. Even so, it is expected to be improved by doping transition elements into Mn_3Ge which enables to engineer the lattice constant with maintaining the crystalline structure [29,30], achieving long-distance in-plane magnetic ordering. In addition, recent study reveals that high pressure induces spin canting along c-axis of the $D0_{19}$ Mn_3Ge, which brings the transformation of the spin configuration to noncoplanar [31]. In our case, a lattice mismatch between Ru and Mn_3Ge possibly induces the pressure to the Mn_3Ge layer. However, our films are polycrystalline with an average grain size of 17.7 nm calculated form distinctive $(20\bar{2}1)$ peak, suggesting that the magnitude of the induced pressure from the mismatch may be small. Even so, such pressure may also be a possible reason to explain low exchange bias and $\langle T_B \rangle$.

In summary, we studied polycrystalline $D0_{19}$ Mn_3Ge films grown on a Ru buffer layer. It was found that post-annealing and substrate heating induce $(20\bar{2}1)$ and (0001) orientations, respectively. These structural characterizations are greatly useful for studying an antiferromagnetic films for device applications such as the exchange bias effect and the giant anomalous Hall effect. Mn-rich Mn_3Ge films show the improvement of the (0001) orientation and result in large H_{ex} up to 61 Oe at 120 K. Although the measured $\langle T_B \rangle$ of 150 K is lower than room temperature, however, further improvements can be expected by doping an additional transition metal to control the lattice constant.

Acknowledgements

This study is partially supported by JSPS-EPSRC Core-to-Core programme (EP/M02458X/1). Also, the auther would like to thank M. Tsunoda and M. Oogane for some comments and J. Gompertz, W. Frost, H. Wu and J. Sinclair for supporting some of the experiments.

References

[1] W.H. Meiklejohn, C.P. Bean, Phys. Rev. 102 (1956) 1413.
[2] B. Dieny, V.S. Speriosu, S. Metin, S.S.P. Parkin, B.A. Gurney, P. Baumgart, D.R. Wilhoit, J. Appl. Phys. 69 (1991) 4774.
[3] https://ec.europa.eu/growth/sectors/raw-materials/specific-interest/critical_en.
[4] H. Kurt, K. Rode, M. Venkatesan, P. Stamenov, J.M.D. Coey, Phys. Status Solidi B 248 (2011) 2338.
[5] H. Kurt, K. Rode, H. Tokuc, P. Stamenov, M. Venkatesan, J.M.D. Coey, Appl. Phys. Lett. 101 (2012) 232402.
[6] A. Hirohata, T. Huminiuc, J. Sinclair, H. Wu, M. Samiepour, G. Vallejo-Fernandez, K. O'Grady, J. Balluf, M. Meinert, G. Reiss, E. Simon, S. Khmelevskyi, L. Szunyogh, R.Y. Díaz, U. Nowak, T. Tsuchiya, T. Sugiyama, T. Kubota, K. Takanashi, N. Inami, K. Ono, J. Phys. D : Appl. Phys. 50 (2017) 443001.
[7] H. Wu, I. Sudoh, R. Xu, W. Si, C.A.F. Vaz, J.-Y. Kim, G. Vallejo-Fernandez, A. Hirohata, J. Phys. D: Appl. Phys. 51 (2018) 215003.
[8] J.F. Qian, A.K. Nayak, G. Kreiner, W. Schnelle, C. Felser, J. Phys. D: Appl. Phys. 47 (2014) 305001.
[9] A. Markou, J.M. Taylor, A. Kalache, P. Werner, S.S.P. Parkin, C. Felser, Phys. Rev. Mater. 2 (2018) 051001.
[10] D. Zhang, B. Yan, S.-C. Wu, J. Kubler, G. Kreiner, S.S.P. Parkin, C. Felser, J. Phys.: Condens. Matter. 25 (2013) 206006.
[11] H. Kurt, N. Baadji, K. Rode, M. Venkatesan, P. Stamenov, S. Sanvito, J.M.D. Coey, Appl. Phys. Lett. 101 (2012) 132410.
[12] A. Sugihara, S. Mizukami, Y. Yamada, K. Koike, T. Miyazaki, Appl. Phys. Lett. 104 (2014) 132404.
[13] N. Kiyohara, T. Tomita, S. Nakatsuji, Phys. Rev. Appl. 5 (2016) 064009.
[14] A.K. Nayak, J.E. Fischer, Y. Sun, B. Yan, J. Karel, A.C. Komarek, C. Shekhar, N. Kumar, W. Schnelle, J. Kübler, C. Felser, S.S.P. Parkin, Sci. Adv. 2 (2018) e1501870.
[15] A.B. Gokhale, R. Abbaschlan, Bullet. Alloy Phase Diagrams 11 (1990) 460.
[16] E. Arras, D. Caliste, T. Deutsch, F. Lançon, P. Pochet, Phys. Rev. B 83 (2011) 174103.
[17] S. Tomiyoshi, Y. Yamaguchi, T. Nagamiya, J. Magn. Magn. Mater. 31 (1983) 629.
[18] I. Dzyaloshinsky, J. Phys. Chem. Solids 4 (1958) 241.
[19] T. Moriya, Phys. Rev. Lett. 4 (1960) 228.
[20] G. Kadar, E. Kren, Int. J. Magn. 1 (1971) 143.
[21] N. Yamada, J. Phys. Soc. Jpn. 59 (1990) 273.
[22] M. Vopsaroiu, M.J. Thwaites, S. Rand, P.J. Grundy, K. O'Grady, IEEE Trans Magn. 40 (2004) 2443.
[23] S. Nakatsuji, N. Kiyohara, T. Higo, Nature 527 (2015) 212.
[24] Z.M. Tian, S. Huang, Y. Qiu, S.L. Yuan, Y.Y. Wu, L. Li, J. Appl. Phys. 113 (2013) 143906.
[25] J. Nogués, I.K. Schuller, J. Magn. Magn. Mater. 192 (1999) 203.
[26] J. Nogués, J. Sort, V. Langlais, V. Skumryev, S. Suriñach, J.S. Muñoz, M.D. Baró, Phys. Rep. 422 (2005) 65.
[27] G. Vallejo-Fernandez, L.E. Fernandez-Outon, K. O'Grady, J. Phys. D: Appl. Phys. 41 (2008) 112001.
[28] K. O'Grady, L.E. Fernandez-Outon, G. Vallejo-Fernandez, J. Magn. Magn. Mater. 322 (2010) 883.
[29] Z.H. Liu, Y.J. Zhang, H.G. Zhang, X.J. Zhang, X.Q. Ma, Appl. Phys. Lett. 109 (2016) 032408.
[30] A. Kundu, S. Ghosh, Intermetallics 93 (2018) 209.
[31] A.S. Sukhanov, L. Sanjay Singh, Th. Caron, A. Hansen, V. Hoser, H. Kumar, A. Borrmann, P. Fitch, K. Devi, C. Felser Manna, D.S. Inosov, Phys. Rev. B 97 (2018) 214402.